Sub-Cycle Dynamics Modeling of IBRs Using LSTM Methods and Synchro-waveform Measurements

Hossein Mohsenzadeh-Yazdi, Fatemeh Ahmadi-Gorjayi, and Hamed Mohsenian-Rad
Department of Electrical and Computer Engineering, University of California, Riverside, CA, USA

***Abstract*—Three novel *data-driven* methods are proposed to model the dynamic response of Inverter-Based Resources (IBRs) to high-frequency sub-cycle disturbances in power systems. Real-world voltage and current waveform data from Waveform Measurement Units (WMUs) are used from a IBR test site in California. The proposed methods are designed based on Long Short-Term Memory (LSTM) networks to capture nonlinear patterns and complex temporal dependencies. They vary in terms of the architecture of the LSTM networks and feature extraction. Experimental results demonstrate significant improvements in the achieved model accuracy, compared to two other recent state-of-the-art data-driven methods in the literature. Furthermore, based on the analysis of *time-synchronized* waveform measurements at two different IBRs, it is shown that the proposed methods have the potential to extend or transfer across different IBRs.**

***Keywords*: Inverter-based resources, data-driven modeling, dynamic response, sub-cycle oscillations, LSTM, clustering, WMU, waveform measurements, synchro-waveforms, real-world data.**

I. Introduction

The dynamic behaviour of modern power systems is increasingly influenced by inverter-based resources (IBRs). Recently, NERC (North American Electric Reliability Corporation) has reported several system-wide incidents that are caused by the unexpected dynamic response of IBRs to transient disturbances [1]. Post-mortem analysis of these incidents has revealed the critical need for high-resolution monitoring of IBRs, particularly during rapid, sub-cycle disturbances. Waveform Measurement Units (WMUs) now offer a solution, providing GPS time-synchronized voltage and current waveform measurements at 64 to 512 samples per cycle [2], [3].

In this paper, we seek to use *real-world* waveform measurements from WMUs at IBRs in a test site in California to develop novel *data-driven* models to predict the dynamic behavior of IBRs in response to *sub-cycle oscillatory* disturbances in power systems. A large number of such sub-cycle oscillations were observed at the IBRs at this test site during the six months period of this study. Of course, other typical forms of disturbances were also present at this site, such as voltage sags and faults. However, we did not consider those disturbances if they did *not* cause sub-cycle oscillations.

A. Literature Review

Physics-based models are traditionally used to model the dynamic behavior of IBRs; e.g., see [4]–[6]. However, they require access to precise models of the internal components and control loops of the IBRs. They may also encounter practical challenges, including computational complexity [7].

A recent alternative to physics-based modeling is to use *data-driven* methods. Some data-driven methods are hybrid. They use field data to identify the parameters of a physical model [8], [9]. Some other methods, such as in [10], do *not* require any knowledge about the physical model of the IBRs. Since the focus in [10] is on phasor measurements, it cannot capture the dynamics of sub-cycle events. The only existing work that utilizes WMU data to model the dynamic response of IBRs is the recent study in [11], where the models are based on modal analysis and regression analysis. As we will show in this paper, our methods outperform the models in [11].

In this paper, our approach involves using Long Short-Term Memory (LSTM) networks [12]. LSTM has *not* been previously used for modeling the sub-cycle dynamic behavior of IBRs. However, it has been used in various other applications in power systems, such as to forecast loads [13], or to forecast solar generation under different weather conditions [14].

B. Summary of Contributions

The contributions in this paper can be summarized as:

1) Three LSTM-based methods are proposed to achieve data-driven models to capture the sub-cycle dynamic behavior of IBRs. *Approach 1* emphasizes extracting the nonlinear relationships and temporal dependencies between sub-cycle differential voltage (input) and sub-cycle differential current (output) at the IBR. *Approach 2* enhances the model by incorporating a new feature to capture the pre-disturbance state of operation of the IBR. *Approach 3* further introduces a clustering pre-processing step to classify and label the IBR's pre-disturbance conditions to be used as a new feature.
2) We show that the basic method in Approach 1 can reduce the average modeling error by 25% and 37%, compared to the two recent state-of-the-art methods in [11], which are based on modal analysis and regression analysis, respectively. The modeling error reduction can reduce to 60% and 67% in Approach 2. With regards to Approach 3, the error reduction is even further, to 85% and 88%, subject to a proper selection of the number of clusters.
3) By making use of the *time-synchronized* waveform measurements, we also investigate the sub-cycle dynamic responses of two different IBRs of the same make, but of different sizes at two different locations, when they both respond to the *same* sub-cycle disturbance in the system. We show that the model that is developed for one IBR can be *reused* to some extent to also capture the

This work is supported in part by CEC grant EPC-16-077. The corresponding author is H. Mohsenian-Rad. E-mail: hamed@ece.ucr.edu.

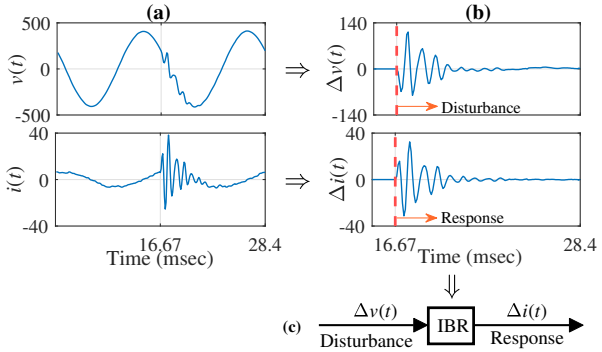

Fig. 1. (a) a sub-cycle voltage oscillation disturbance, which in turn causes agitation in the injected current by the IBR; (b) the corresponding differential waveforms; (c) a data-driven model for the input-output relationship between the sub-cycle disturbance and the sub-cycle response of the IBR.

sub-cycle dynamic response of the other IBR, subject to making some minor adjustments in the original model.

The analysis in this paper is based on *real-world waveform measurements*. No computer simulations is used in this paper.

II. Problem Statement

Consider Fig. 1(a), which shows the *real-world* waveform measurements that are captured by a WMU at one phase of a three-phase PV unit in California during a system-wide disturbance. The voltage and current waveform measurements are denoted by $v(t)$ and $i(t)$, respectively. The disturbance causes a *voltage oscillation event* for a short period of time (less than half of an AC cycle). This in turn causes a *dynamic response* in the PV inverter's current, which is oscillatory and transient. Our goal is to model this dynamic response, by solely using the waveform measurements at the IBR, without access to the internal physical models of the IBR components.

Next, consider Fig. 1(b). It shows the *differential waveforms* corresponding to the raw voltage and current waveform measurements in Fig. 1(a). Given a waveform $x(t)$, its corresponding differential waveform is obtained as [15, Section 4.2.5]:

$$\Delta x(t) = x(t) - x(t-T), \quad \forall\, t \geq t_0, \tag{1}$$

where t_0 is the start time of the event and $T = 1/60$ seconds denotes the interval of the waveform. As we can see in Fig. 1(b), the differential waveforms provide clear signatures of the sub-cycle disturbance and the sub-cycle response of the IBR.

Finally, consider Fig. 1(c). It shows the input-output relationship between $\Delta v(t)$ as the input time-series and $\Delta i(t)$ as the output time-series. Our goal is to develop methods based on LSTM to model the above input-output relationship.

III. Approach 1: Basic LSTM Model

LSTM is a powerful tool for analyzing time-series. It can learn complex temporal dependencies and nonlinear patterns. In this section, we introduce our first model based on LSTM.

A. LSTM Architecture and Methodology for Approach 1

Fig. 2 illustrates the overall architecture of the LSTM model in Approach 1. The input to this model is a window of length *lag* of the most recent samples of the time-series of

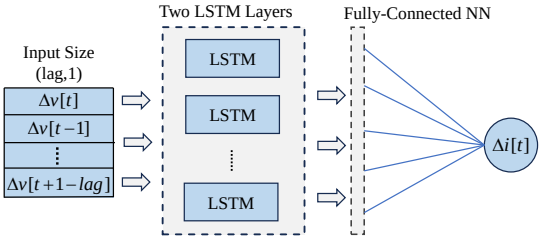

Fig. 2. Architecture of the proposed LSTM model in Approach 1.

the differential voltage waveform. The output of this model is the present sample of the time-series of the differential current waveform. Note that, while notations $\Delta v(t)$ and $\Delta i(t)$ denote the entire time series of the differential waveform measurements, notations $\Delta v[t]$ and $\Delta i[t]$ denote the samples of these two time-series at any given time t. If there are N samples in the differential voltage and the differential current, then there will be N windows of length *lag*, traversing the input signal, sample by sample, from left to right, in order to reconstruct the entire current waveform response of the IBR.

The main objective of the LSTM model in Approach 1 is to discern the relationship between each window of the most recent samples in the input time-series and its corresponding output. This relationship can be expressed as follows:

$$\Delta i[t] \;=\; f\big(\Delta v[t],\, \Delta v[t-1],\, ...,\, \Delta v[t+1-lag]\big), \tag{2}$$

where we seek to identify the optimal choice of function $f(\cdot)$.

It is worth nothing that, prior to constructing the windows of the input signal, the event data is partitioned into two sets: training events and test events. Following the construction of the input windows for all training events, the windows, along with their corresponding outputs, are *shuffled* and further *split* into training and validation data. This process guarantees a diverse representation of the dynamics of the system across different events, in both training and validation datasets.

The LSTM model in Fig. 2 incorporates two LSTM layers. Each LSTM cell has three gating mechanisms [12]: input gate, forget gate, and output gate, as shown below, respectively:

$$\begin{aligned} i[t] &= \sigma(W_{ii}x[t] + b_{ii} + W_{hi}h[t-1] + b_{hi}),\\ f[t] &= \sigma(W_{if}x[t] + b_{if} + W_{hf}h[t-1] + b_{hf}),\\ o[t] &= \sigma(W_{io}x[t] + b_{io} + W_{ho}h[t-1] + b_{ho}), \end{aligned} \tag{3}$$

where x_t is the input at time t and $h[t-1]$ is the hidden state from the previous time step. The weight matrices W and bias vectors b are parameters that are learned during the training process. The gates in (3) are controlled by sigmoid activation functions $\sigma(\cdot)$, which generate values between 0 and 1, determining the flow of information through the cell. A *tanh* activation function is applied to the candidate cell state:

$$g[t] = \tanh(W_{ig}x[t] + b_{ig} + W_{hg}h[t-1] + b_{hg}), \tag{4}$$

allowing the model to capture long-term dependencies. The cell state that represents the long-term memory is modified by the input gate, forget gate, and candidate cell state as

$$c[t] = f[t]c[t-1] + i[t]g[t]. \tag{5}$$

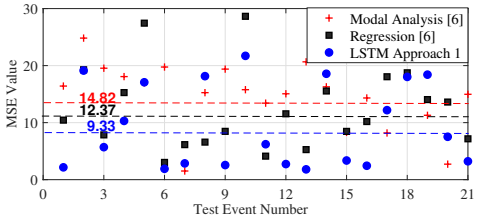

Fig. 3. Individual MSE values (and their averages in the dashed lines) for the proposed LSTM model in Approach 1 in comparison with the state-of-the-art modal analysis and regression analysis models in [11] for all Test Events.

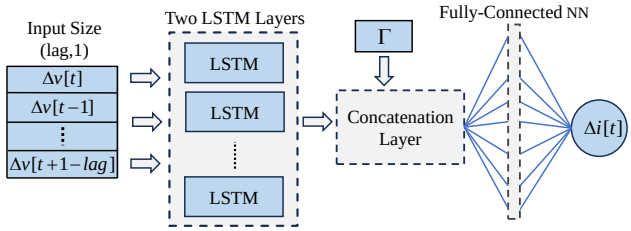

Fig. 4. Architecture of the proposed LSTM model in Approach 2.

The hidden state that serves as the short-term memory is calculated using the output gate and the current cell state as:

$$h[t] = o[t]\tanh(c[t]). \tag{6}$$

Subsequently, a layer of a fully connected neural network serves as the last layer in the LSTM networks architecture in Fig. 2, generating the ultimate output of the network.

In Approach 1, the hyperparameters were set manually with the commonly used values. The LSTM layers are initialized with 64 units. The final Dense layer with 1 unit and a ReLU activation function produces the output. The model is trained using Adam optimizer (learning rate of 0.01) over the MSE loss function. Thirty percent of the training data is used for validation. The TensorFlow's Keras API was used to build the LSTM network, with its default random weight initialization.

B. Experimental Results and Performance Comparison

In this section, we compare Approach 1 with the Modal Analysis method and the Regression Analysis method in [11]. To have a fair comparison, we use the exact same real-world training and testing data sets in [11]. Specifically, we used waveform measurements from a WMU at a 480 V / 100 kW PV unit over a six-month period. This dataset included 63 instances of sub-cycle system-wide disturbances, and the corresponding responses of the IBR. As in [11], we designated 42 disturbances for training and 21 disturbances for testing.

The randomness inherent in the training of the LSTM model is addressed by conducting 40 iterations of training and taking the average. This helps mitigate the influence of stochastic variations, ensuring a more robust and representative analysis.

The results are shown in Fig. 3. Here, we show the Mean Square Error (MSE) for each method on each of the 21 test cases. The horizontal dashed lines show the average MSE for each method. Notice that, while the average MSE values for the Modal Analysis and the Regression Analysis are 14.82 and 12.37, respectively, the proposed LSTM method in Approach 1 significantly reduces the average MSE value down to 9.33, which indicates 37% and 25% improvements compared to Modal Analysis and Regression Analysis, respectively.

IV. Approach 2: LSTM Model with Additional Feature Layer on Pre-Event Conditions

Our second approach is motivated by the results that we previously saw in Fig. 3. On average, the MSE values for the LSTM model in Approach 1 demonstrated a significant improvement while some of the test cases still had high MSE values, as high as 20. Upon comparing the differential voltage waveforms, we observed test cases where the two test events had *almost identical* differential voltage waveforms, yet they showed *significant differences* in their MSE values.

After further examination, our conjecture was that the cause of the poor performance of Approach 1 in certain test cases is the differences in their *pre-event operating conditions*. This refers to the extent of the IBR being in steady-state versus being in volatile conditions, shortly *before* the event occurs.

In this regard, we can treat not only the recent method in [11] but also our own method in Approach 1 as *two baselines* to evaluate the performance of Approach 2 and Approach 3.

A. LSTM Architecture and Methodology for Approach 2

To incorporate the pre-event condition to examine the above conjecture, we focused on the characteristics of the differential current waveform at the cycle *immediately before* the start of the event. The differential current waveform in the cycle immediately before the start of the event can be obtained as

$$\Delta i[t_0 - T - 1 : t_0 - 1]. \tag{7}$$

If all the samples in (7) are zero, then the IBR was in a truly *steady-state* condition. If there are several non-zero and large samples in (7), then the IBR's operation was *not* in a steady-state condition; because the consecutive cycles had significant differences *even before* the voltage oscillation event happens.

Hence, we consider the following *new feature* as a *new input* to the model to indicate the pre-event condition of the IBR:

$$\Gamma = \|\Delta i[t_0 - T - 1 : t_0 - 1]\|_2. \tag{8}$$

A large Γ indicates that the *pre-event conditions* at the IBR was far from steady-state, such as due to a recent event that is still affecting the behavior of the IBR, or due to an internal dynamic in the IBR that has not yet reached its steady state.

Accordingly, we proposed a new architecture for the LSTM model, as in Fig. 4. This new architecture directly incorporates Γ as a new feature (new input). To leverage this new input, a *concatenation layer* is introduced, positioned between the second LSTM layer and the final layer of the fully-connected neural network. The input size to this new layer is equal to the output size of the second LSTM layer plus one, and its output size is equal to the input size of the last layer.

In Approach 2, most of the LSTM parameters are similar to Approach 1, except for the new concatenation layer. This new layer has 64 units and employs a rectified linear unit (ReLU) activation function to process the combined information.

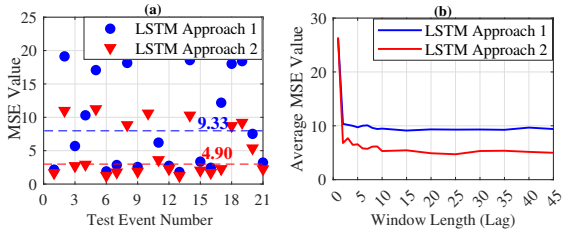

Fig. 5. Comparing Approach 1 and Approach 2: (a) the MSE values for each test case; (b) the average MSE values versus the changes in the *lag* parameter.

B. Experimental Results and Performance Comparison

The results for comparing Approach 2 with Approach 1 are shown in Fig. 5(a). Approach 2 outperforms Approach 1 in *every* test case. On average, the MSE reduces from 9.33 to 4.90. These results are 67% and 60% better than the Modal Analysis and the Regression Analysis methods, respectively. In essence, Γ captures the *operating conditions* of the system during each event. Hence, including Γ as a feature results in improving the performance in our data-driven models.

Importantly, the above superior results for Approach 2 are *not* sensitive to the choice of the LSTM parameters. For example, regardless of the choice of the *lag*, the average MSE is always much lower for Approach 2 than Approach 1.

V. Approach 3: LSTM Model Based on Combining Approach 2 with Feature Clustering

As we saw in Approach 2, considering Γ as a new feature can incorporate the pre-event operating conditions of the IBR into the LSTM model to enhance its performance. In this section, we incorporate the pre-event conditions in a different way, by *clustering* the events based on their values of Γ, to represent each event based on the type of its pre-event conditions. This was motivated by our observation that there are similarities in the dynamic behavior of the IBR during the events that have similar Γ. Therefore, a grouping of the events based on Γ may help to improve the model's performance.

A. LSTM Architecture and Methodology for Approach 3

Fig. 6 illustrates the architecture of the LSTM model in Approach 3. Compared to the architecture of Approach 2 in Fig. 4, we added a *clustering module* between input Γ and the concatenation layer, to turn the raw value of Γ into a *label* based on the cluster number of the event according to Γ.

Clustering is done using K-means clustering. The number of clusters is set by parameter K. The *unsupervised* nature of the clustering process is a critical aspect in this approach in order to eliminate the need for any prior classification knowledge with regards to the pre-event conditions.

B. Experimental Results and Performance Comparison

Table I provides a comparison between Approach 3 and Approaches 1 and 2, for different choices of K. We can see that the average MSE can reduce to as low as 1.85 when $K = 4$. This is a major improvement even compared to Approach 2. In fact, the average MSE in this case is 88% and 85% less than the Modal Analysis, Regression Analysis, respectively.

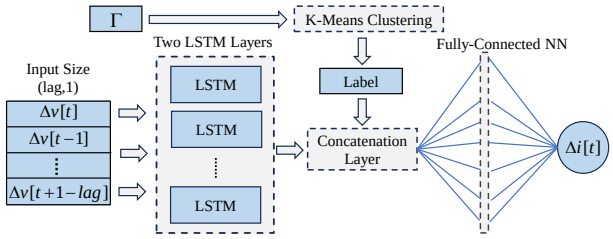

Fig. 6. Architecture of the proposed LSTM model in Approach 3.

TABLE I
Performance of Approach 3 for Different Number of Clusters K in Comparison with Approach 1 and Approach 2

Method	Approach 1	Approach 2	Approach 3				
			K=2	K=3	K=4	K=5	K=6
Average MSE	9.33	4.90	9.93	3.92	**1.85**	7.70	3.00

However, it appears that the results in Approach 3 are sensitive to the choice of K. Hence, while it is evident that there is great potential in Approach 3 to benefit from a clustering module, more research is needed in the future to identify an unsupervised process to properly choose K.

VI. Using Synchro-waveforms to Model the Dynamic Response of Multiple IBRs

For the analysis in this section, we installed a second WMU at the location of a second IBR on the same network, to take advantage of *time-synchronized* waveform measurements in the context of this paper. IBR 2 is made by the same manufacturer but has a larger rated power and is connected to a larger array of solar panels. It is also on a *different feeder*.

Accordingly, we were able to observe how the two IBRs *simultaneously* respond to the *same* sub-cycle voltage oscillation events. An example is shown in Fig. 7(a), where we plotted the *time-synchronized* raw voltage and raw current waveforms at the two IBRs. We can see that the voltage disturbances are very similar at the two locations. The dynamic responses of the two IBRs, which are manifested in their current waveforms, are also generally similar, but at *different magnitudes*. Another key observation in Fig. 7(a) is the presence of higher distortions in the current waveforms at IBR 2 than IBR 1, in the cycles before the start of the event. Fig. 7(b) shows the differential waveforms corresponding to the measurements in Fig. 7(a).

Inspired by the above observations, we collected 12 new test events that were captured by *both* WMUs at the two IBRs. *All these test events are new*, i.e., they are different from the 21 test events in Sections III, IV, and V. We applied the LSTM model in Approach 2 to the new 12 test events. The average MSE value was obtained at 4.69 for IBR 1. This further confirms the robust performance of Approach 2; because the results highly resemble the previous results in Section IV.

Next we applied the model that was developed for IBR 1 in Section IV to the data from IBR 2. The results are shown in Fig. 8, where we plotted the average MSE across all the 12 new test events at IBR 2, versus a *scaling parameter*, denoted by λ. In our analysis, we use parameter λ as follows:

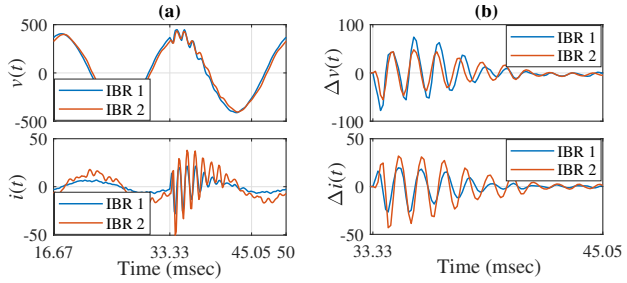

Fig. 7. Time-synchronized waveform measurements at two different IBRs during the same sub-cycle voltage oscillation disturbance: (a) the raw waveform measurements; (b) the corresponding differential waveforms.

- First, we *divide* Γ from IBR 2 by scaling factor λ to make it comparable to Γ in IBR 1. Then we apply the model from Approach 2 from IBR 1 to the data from IBR 2.
- Once the dynamic response is estimated from the model, we *multiply* the resulting differential current waveform by λ to make the results applicable to IBR 2.

From the results in Fig. 8, the best performance is achieved at $\lambda = 1.7$, which is very close to the *ratio* of the rated capacity of IBR 2 to the rated capacity of IBR 1, which is 1.8.

The best average MSE value for IBR 2 in Fig. 8 is 14.63. While this is not as good as the results that we obtained for IBR 1 in Section IV, it is at the same level of accuracy that was obtained in [11] for IBR 1 using Modal Analysis. This is a surprisingly high accuracy, given the fact that the model was developed based on the data from IBR 1, yet it was applied nicely to the data from IBR 2 with very minor changes.

While we cannot make any major claim about the analysis across IBR 1 and IBR 2, the above results are promising to inspire future research to investigate the ability to extend (or transfer) the proposed data-driven models across different IBRs with no or little changes, using synchronized waveform measurements. In the future, we may enhance the accuracy in such model transfers by developing a series of LSTM-based representative models for each type of IBRs from a larger population of IBRs. Combining LSTM with techniques from transfer learning may also be useful in this line of work.

VII. Conclusions

Three LSTM-based methods were proposed to use waveform measurements from WMUs to model the dynamic behavior of IBRs in response to sub-cycle oscillatory disturbances. The performance of the methods were evaluated using real-world waveform data. The methods can significantly reduce the modeling error, to half or less, compared to the state-of-the-art methods based on modal analysis and regression. By using time-synchronized waveform measurements from two IBRs, it was shown that the methods have the potential to be reused (transferred) across different IBRs. In the future, we can expand our analysis to consider other types of disturbances, such as voltage sags and different faults. Another direction for future work is to optimally tune the hyperparameters of the LSTM model. We also intend to enhance performance evaluation by conducting sensitivity analysis, cross validation, and different groupings of training and test samples assessments.

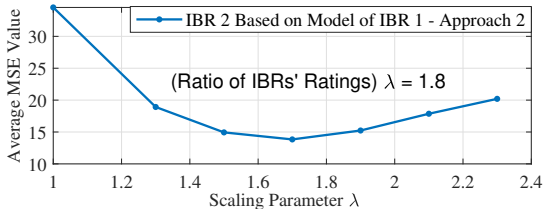

Fig. 8. The results for applying the model (Approach 2) from IBR 1 to the time-synchronized waveform data at IBR 2 using different scaling factors.

The findings in this paper can help utilities and independent system operators (ISOs) to enhance their situational awareness and improve stability and reliability of their networks. First, our models can be used for condition monitoring and diagnostics at IBRs. Apart from comparing the behavior of similar IBRs to identify abnormal dynamics, we can use our methods to detect any significant changes in the dynamic behavior of each IBR, indicating potential failures that may require inspection. Second, our models can be used in developing digital twins for IBR, predicting their responses to power system disturbances, and preventing undesirable tripping. Third, the analysis is this paper can be employed to compare the dynamic responses of a group of IBRs in a region, to predict any ripple effects that may follow system-wide disturbances and potential agitations in power production or momentary IBR secession.

References

[1] North American Electric Reliability Corporation, "Multiple Solar PV Disturbances in CAISO," NERC Report, Apr. 2022.
[2] A. Silverstein and J. Follum, "High-resolution time-synchronized grid monitoring devices," NASPI Report NASPI-2020-TR-004, Mar. 2020.
[3] H. Mohsenian-Rad and W. Xu, "Synchro-waveforms: A window to the future of power systems data analytics," *IEEE Power and Energy Magazine 21*, vol. 21, no. 5, pp. 68–77, Sep 2023.
[4] M. Abido and M. Khalid, "Seven-parameter PV model estimation using differential evolution," *Electrical Eng.*, vol. 100, pp. 971–981, 2018.
[5] P. P. Dash and M. kazerani, "Dynamic modeling and performance analysis of a grid-connected current-source inverter-based photovoltaic system," *IEEE Trans. on Sustainable Energy*, vol. 2, pp. 443–450, 2011.
[6] M. Ghazavi Dozein, B. C. Pal, and P. Mancarella, "Dynamics of inverter-based resources in weak distribution grids," *IEEE Trans. on Power Systems*, vol. 37, pp. 3682–3692, Jan 2022.
[7] H. Cai, J. Xiang, and W. Wei, "Modelling, analysis and control design of a two-stage photovoltaic generation system," *IET Renewable Power Generation*, vol. 10, no. 8, pp. 1195–1203, June 2016.
[8] W. Li, P. Chao, X. Liang, J. Ma, D.Xu, and X. Jin, "A practical equivalent method for DFIG wind farms," *IEEE Trans. on Sustainable Energy*, vol. 9, no. 2, pp. 610–620, Apr 2018.
[9] L. Fan, Z. Miao, S. Shah, P. Koralewicz, V.Gevorgian, and J. Fu, "Data-driven dynamic modeling in power systems: A fresh look on inverter-based resource modeling," *IEEE Power & Energy Magazine*, Jun 2022.
[10] P. Khaledian and *et al.*, "Event-based dynamic response modeling of large behind-the-meter solar farms: A data-driven method based on real-world data," in *Proc. of the IEEE PES ISGT*, Washington, DC, Jan 2023.
[11] F. Ahmadi-Gorjayi and H. M. Rad, "Data-driven models for sub-cycle dynamic response of inverter-based resources using WMU measurements," *IEEE Trans. on Smart Grid*, vol. 14, pp. 4125–4128, Sep 2023.
[12] S. Hochreiter and J. Schmidhuber, "Long short-term memory," *Neural computation*, vol. 9, no. 8, pp. 1735–1780, 1997.
[13] W. Kong, Z. Y. Dong, Y. Jia, D. J. Hill, Y. Xu, and Y. Zhang, "Short-term residential load forecasting based on lstm recurrent neural network," *IEEE Trans. on smart grid*, vol. 10, no. 1, pp. 841–851, 2017.
[14] M. Abdel-Nasser and K. Mahmoud, "Accurate photovoltaic power forecasting models using deep lstm-rnn," *Neural computing and applications*, vol. 31, pp. 2727–2740, 2019.
[15] H. Mohsenian-Rad, *Smart Grid Sensors: Principles and Applications*. Cambridge University Press, United Kingdom, Apr. 2022.